Analogue closed-loop optogenetic modulation of hippocampal pyramidal cells dissociates gamma frequency and amplitude

Elizabeth Nicholson[*1], Dmitry A Kuzmin[*1], Marco Leite[1], Thomas E Akam[2,3] and Dimitri M Kullmann[1]

[1]UCL Institute of Neurology, University College London, WC1N 3BG, United Kingdom

[2]Champalimaud Neuroscience Program, Champalimaud Center for the Unknown, Portugal

[3]Department of Experimental Psychology, University of Oxford, United Kingdom (present address)

*****These authors contributed equally

Correspondence to D.M. Kullmann (d.kullmann@ucl.ac.uk)

Abstract

Gamma-band oscillations are implicated in modulation of attention, integration of sensory information and flexible communication among anatomically connected brain areas. How networks become entrained is incompletely understood. Specifically, it is unclear how the spectral and temporal characteristics of network oscillations can be altered on rapid timescales needed for efficient communication. We use closed-loop optogenetic modulation of principal cell excitability in mouse hippocampal slices to interrogate the dynamical properties of hippocampal oscillations. Gamma frequency and amplitude can be modulated bi-directionally, and dissociated, by phase-advancing or delaying optogenetic feedback to pyramidal cells. Closed-loop modulation alters the synchrony rather than average frequency of action potentials, in principle avoiding disruption of population rate-coding of information. Modulation of phasic excitatory currents in principal neurons is sufficient to manipulate oscillations, suggesting that feed-forward excitation of pyramidal cells has an important role in determining oscillatory dynamics and the ability of networks to couple with one another.

Impact statement

Neurons can synchronize, supporting flexible communication among brain areas; closed-loop optogenetics allows the frequency and power of population oscillations to be dissociated, providing a tool to interrogate how networks couple.

Introduction

Gamma-band (approximately 30 to 120 Hz) oscillations have been implicated in the modulation of attention and perception, in action initiation, spatial navigation and memory encoding, and have also been proposed to underlie flexible information routing among anatomically connected regions (Akam & Kullmann, 2010, 2014; Börgers & Kopell, 2003; Fries, 2005; Kirst, Timme, & Battaglia, 2016; Lisman, 2010; Rodriguez et al., 1999; Salinas & Sejnowski, 2001; Schnitzler & Gross, 2005). Central to several of these proposed roles is the ability of gamma oscillations in different areas to enter into, and exit, states of synchrony with one another (Akam, Oren, Mantoan, Ferenczi, & Kullmann, 2012; Fries, 2015; Varela, Lachaux, Rodriguez, & Martinerie, 2001). Evidence for behavioural-state dependent coupling and uncoupling comes from variable oscillatory coherence among distinct components of the visual cortex, correlating with selective stimulus attention (Bosman et al., 2012; Grothe, Neitzel, Mandon, & Kreiter, 2012). An earlier study in the rodent hippocampal formation showed that the CA1 subfield can flip between a state of coherence with the medial entorhinal cortex at ~110 Hz and a state of coherence with the CA3 subfield at ~40 Hz, correlating with information flow through the temporo-ammonic and Schaffer collateral pathways respectively (Colgin et al., 2009). Although several experimental confounds cloud the interpretation of coherence measured from local field potential (LFP) recordings (Buzsáki & Schomburg, 2015), these studies provide some of the most compelling evidence that gamma-band oscillatory entrainment underlies flexible functional connectivity.

Although the cellular mechanisms underlying gamma oscillations have been extensively studied (Bartos, Vida, & Jonas, 2007; Buzsáki & Wang, 2012), there remain uncertainties over the fundamental determinants of their dynamics and the relative contributions of excitatory and inhibitory signalling. Gamma-band oscillations can be induced *in vitro* in the presence of blockers of ionotropic glutamate receptors (Whittington, Traub, & Jefferys, 1995), or *in vivo* by optogenetic stimulation of parvalbumin-positive interneurons (Cardin et al., 2009; Sohal, Zhang, Yizhar, & Deisseroth, 2009), underlining the importance of fast perisomatic inhibition (Bartos et al., 2002; Fisahn et al., 2004; Mann, Radcliffe, & Paulsen, 2005). Robust population oscillations can also be simulated in exclusively inhibitory networks (Wang & Buzsáki, 1996). These experimental and computational observations emphasize the importance of inhibitory kinetics. Nevertheless, gamma-band oscillations can be entrained by sinusoidal optogenetic stimulation of pyramidal neurons in an *in vitro* hippocampal slice preparation (Akam et al., 2012). This observation implies that phasic depolarization of principal cells can determine the gamma rhythm and argues against a model where the only role of pyramidal cells is to tonically depolarize a network of reciprocally coupled interneurons (Bartos et al., 2007; Tiesinga & Sejnowski, 2009).

Further insight into the dynamical mechanisms of synchronization between oscillating networks comes from examining the phase response curve (PRC) of the network oscillation, defined as the phase advance or delay produced by a transient stimulation, as a function of the instantaneous phase at which the stimulus is delivered. The finding that gamma in an *in vitro* hippocampal slice preparation shows a biphasic PRC (Akam et al., 2012) is consistent with the hypothesis that this oscillation can be entrained by appropriately modulated afferent activity. The shape of the PRC is furthermore accurately reproduced with a simple neural mass model (Wilson & Cowan, 1972), where extracellular electrical or optogenetic stimuli are represented as transient perturbations of the instantaneous level of excitation or inhibition (Akam et al., 2012). Recent theoretical work has derived population PRCs for oscillations in spiking network models, providing an insight into how mechanisms of oscillation generation determine entrainment properties (Akao, Ogawa, Jimbo, Ermentrout, & Kotani, 2018; Kotani, Yamaguchi, Yoshida, Jimbo, & Ermentrout, 2014). Nevertheless, there remains a large gap between the PRC and understanding the determinants of the oscillatory frequency and interactions between gamma-generating circuits.

The present study investigates the dynamical properties of gamma oscillations by using closed-loop optogenetics to create an artificial feedback loop between the oscillatory network activity (as assessed by the LFP) and excitatory input to the principal cell population. Specifically, we delivered analogue-modulated excitation whose strength was a function of the instantaneous phase and amplitude of the oscillation. This approach is quite distinct from previous closed-loop applications of optogenetics (Grosenick, Marshel, & Deisseroth, 2015), which have adopted one of four main strategies. First, several studies have used the detection of a change in the state of a network, such as the onset of an electrographic seizure (Krook-Magnuson, Armstrong, Oijala, & Soltesz, 2013; Paz et al., 2013) or sharp-wave ripple (Stark et al., 2014), to trigger light delivery and return the network to its ground state. Second, light pulses have been timed according to the phase of a theta oscillation (Siegle & Wilson, 2014), while examining the consequences for behaviour. In the latter example the theta oscillation itself was not altered. Third, optogenetics has been used to regulate the overall activity of a population of neurons at a desired level (Newman et al., 2015). Fourth, optogenetic depolarization of interneurons, triggered by spikes in an individual principal cell, has been used to simulate a feedback inhibitory loop to interrogate their role in gamma (Sohal et al., 2009; Veit, Hakim, Jadi, Sejnowski, & Adesnik, 2017). The goal of the present investigation is qualitatively different: to understand how the spectral characteristics of gamma are affected by rhythmic excitation arriving at different phases. Computational simulations have suggested that closed loop optogenetics could be used to adjust the phase

of gamma (Witt et al., 2013), but whether it can alter its frequency or amplitude remains unclear.

Results

Closed-loop feedback modulation of affects gamma oscillations in CA1

We expressed the red-shifted optogenetic actuator C1V1 (Yizhar et al., 2011) in the mouse hippocampus CA1 under the *Camk2a* promoter to bias expression to excitatory neurons. The local field potential (LFP) was recorded in the CA1 pyramidal cell layer in acute hippocampal slices. A slowly increasing ramp of light (peak wavelength 590 nm) was delivered via a light-emitting diode (LED) coupled to the epifluorescence port of an upright microscope, eliciting a gamma oscillation (**Fig. 1a, b**), as previously reported in rodents (Adesnik, 2018; Adesnik & Scanziani, 2010; Akam et al., 2012; Butler, Mendonça, Robinson, & Paulsen, 2016; Pastoll, Solanka, van Rossum, & Nolan, 2013), cats (Ni et al., 2016) and monkeys (Lu et al., 2015).

In order to investigate the role of phasic excitation in setting the dynamical properties of gamma we used the LFP itself to manipulate the optogenetic drive in real time. The LED driver command was multiplied by a simple function of the instantaneous value of the LFP and its time-derivative: $(1 + k_1 \text{LFP} + k_2 d\text{LFP}/dt)$, where k_1 and k_2 are positive or negative constants. These operations were implemented with a field-programmable gate array (FPGA) and applied for a defined duration (typically 1 or 2 seconds) during the ramp. This yielded a change in the spectral properties of the oscillation, which lasted for the duration of the closed-loop feedback (**Fig. 1c**). Because both the LFP and its time-derivative fluctuated about 0, the “gamma clamp” had little effect on the average illumination intensity relative to an unmodulated ramp. Changes in the oscillation frequency or power could therefore not be attributed to a net increase or decrease in the average optogenetic drive to pyramidal neurons.

We adjusted the clamp function by altering the values of k_1 and k_2 and asked whether the frequency and/or power of the gamma oscillation can be modulated bidirectionally. Changes in spectral properties were related to the phase difference between the LFP and the LED drive during the clamp, as estimated from the cross-spectrum at maximal magnitude. In-phase modulation, achieved by setting k_1 positive and $k_2 = 0$, led to an increase in oscillatory power and frequency (**Fig. 2a**). Modulating the ramp in anti-phase relative to the LFP, by

setting k_1 negative, led to a decrease in both frequency and power (**Fig. 2b**). Advancing the phase of the clamp by approximately 90°, achieved by setting $k_1 = 0$ and k_2 positive, increased the frequency of the oscillation whilst decreasing is power (**Fig. 2c**). Finally, a decrease in frequency and increase in power was achieved by delaying the trough of the clamp modulation relative to the LFP, by setting k_2 negative (**Fig. 2D**). Detailed inspection of the ramp command waveform during the clamp shows that it was in some cases distorted relative to the LFP, as expected from its non-sinusoidal shape (Cole & Voytek, 2017) (e.g. **Fig. 2c, d**), and so the LED-LFP phase differences were only approximate.

Attempts to estimate the instantaneous oscillation phase, for instance using a Hilbert transform, and to use this to phase-advance or phase-delay a template of the LFP, compressed or stretched in time, were unsuccessful: the phase jitter and cycle-to-cycle variability in the amplitude and frequency of the gamma oscillation (see LFP traces in Fig. 2) prevented accurate estimation of these parameters in the face of closed loop feedback.

Oscillation clamp is broadly consistent with the phase response curve of gamma

Changes in frequency and power, expressed in relation to the approximate phase difference between the LED command and the LFP, were qualitatively consistent across experiments (**Fig. 3a–c**). Moreover, as the LED-LFP phase difference was rotated through a complete cycle, the effect on the oscillation in the two-dimensional plane defined by the change in oscillation frequency and power also rotated through 360°, such that with the appropriate phase of closed-loop feedback the network oscillation could be pushed in any desired direction in the oscillation frequency-power space (**Fig. 3c)**.

To gain a mechanistic insight, we asked if the characteristic relationship between the frequency change and the LED-LFP phase difference could be explained by the shape of the phase-response curve (PRC) previously reported (Akam et al., 2012). In that study, a brief ‘kick’ was applied on top of the LED ramp command, and the phase advance or delay of subsequent oscillations was related to the phase of the LFP at which the transient occurred. A phase delay was observed when the transient optogenetic stimulus was delivered at the trough of the LFP, when pyramidal neurons are most likely to fire. The maximal phase advance, in contrast, occurred when the stimulus was delivered approximately one third of a cycle after the trough of the LFP. Assuming linear behaviour, the effect of modulating the light intensity in closed loop can be obtained by averaging the product of the phase shift and the LFP over the entire cycle of the oscillation. The circular cross-correlogram between the typical LFP shape and the PRC should then predict the

effect of modulating the optogenetic drive by the shape of the LFP itself at arbitrary degrees of phase advance or delay (**Fig. 3d**). In-phase modulation is expected, on the basis of this calculation, to phase-advance the oscillation, and thus to result in an increase in oscillatory frequency over successive cycles. Anti-phase modulation, in contrast, is predicted to phase-delay the oscillation, and thus to decrease is frequency. The circular cross-correlation is, moreover, asymmetrical, broadly consistent with the shape of the relationship between the change in frequency and LED-LFP phase difference observed in the clamp experiments (**Fig. 3a**).

Although the shape of the PRC is consistent with the changes in gamma frequency achieved with closed loop modulation at different LED-LFP phase differences, on its own it says nothing about changes in power. Power was maximally decreased with a phase advance of the LED command over the LFP around 90°, whilst it was maximally increased with a phase delay around 90° (**Fig. 3b**). The relative phases at which frequency and power were altered are however consistent with the behaviour of a normal form description of a super-critical Hopf bifurcation in the vicinity of its limit-cycle. In this scenario, the LFP would approximate an observed variable, and the optogenetic drive would act in the direction of a hidden variable at a +90° angle to the LFP.

A deeper understanding of the characteristic changes in frequency and power of the LFP with different LED-LFP phase differences require an insight into how neurons spike and ultimately how membrane currents respond to the fluctuations in optogenetic drive. We therefore performed single-cell recordings in parallel with the LFP recordings.

Gamma clamp affects the timing, not rate, of pyramidal neuron firing

Although the average illumination intensity was not altered during the gamma clamp, for certain LED-LFP phase relationships gamma power increased or decreased robustly. Inhibitory currents in principal neurons, rather than spikes or excitatory currents, have previously been shown to be the main determinant of the LFP (Oren, Hájos, & Paulsen, 2010), suggesting that the change in power during the clamp is not a direct effect of the optogenetic drive but results instead from a change in pyramidal neuron synchrony or phase, in a reciprocal relationship with the degree and temporal synchrony of interneuron recruitment. To determine how the clamp affects pyramidal neuron firing, we repeated experiments with an additional patch pipette to record from individual pyramidal neurons in cell-attached mode. Individual action potentials were used to align the simultaneously recorded LFP, and to estimate the phase at which they occurred. During an unmodulated

ramp, pyramidal cells tended to spike sparsely, close to the trough of the oscillation, consistent with previous studies of pharmacologically induced oscillations (Fisahn, Pike, Buhl, & Paulsen, 1998). During the clamp, an increase in oscillatory power was associated with a corresponding increase in the degree of synchrony of pyramidal cell firing: the circular dispersion of LFP phase at which pyramidal cells fired decreased relative to the unclamped situation (**Fig. 4a**). Conversely, a decrease in power was accompanied by a relative desynchronization of pyramidal cell firing. This relationship was qualitatively consistent, as indicated by the change in vector length obtained from the circular average of spike phases (**Fig. 4c**). The vector length increased when oscillation power increased ($p = 0.02$, $n = 12$, sign test), and decreased when oscillation power decreased ($p = 0.025$, $n = 5$). Strikingly, however, there was no change in the overall firing rate of pyramidal cells when the oscillation power was increased or decreased by the clamp. Changes in power were thus achieved by tightening the synchrony of firing, or by desynchronizing action potentials, rather than by altering the overall activity of pyramidal neurons.

Increases in oscillatory frequency were accompanied by a phase advance of pyramidal cell firing relative to the LFP (**Fig. 4b, c,** $p = 8 \times 10^{-7}$, $n = 7$, Hotellier test (Zar, 2009)). A trend for a phase delay was observed in a small number of experiments where frequency-lowering clamp was tested ($n = 3$). This observation is consistent with the view that changes in the phase of pyramidal neuron action potentials are causally upstream of changes in gamma frequency, even though the current generators of the LFP itself are dominated by GABAergic signalling (Gulyás et al., 2010; Hájos et al., 2004; Oren et al., 2010).

Excitatory current phase in principal cells determines changes in gamma spectral properties

In the examples illustrated in **Figs. 4a** and **b**, the optogenetic modulation was applied with a phase advance over the LFP of ~0° and ~45° respectively. Why does in-phase modulation result in an increase in power, and phase-advanced modulation result in an increase in frequency? To gain a mechanistic insight into how gamma clamp operates, we examined the phase of excitation experienced by pyramidal neurons during different clamp regimes.

We repeated experiments as above, but with one pipette used to voltage–clamp a pyramidal neuron at the estimated $GABA_A$ reversal potential (approximately –70 mV), and the other pipette to record the LFP. We then measured the inward current at each phase of the gamma oscillation, as defined by the LFP, and repeated this over consecutive cycles to obtain an average time-course (**Fig. 5a**). The minimum (that is, least negative) inward

current during the average cycle was subtracted to yield an estimate of the phasic excitatory current, which could then be represented as a vector representing its average phase and amplitude (**Fig. 5b**). During unclamped gamma, the excitatory current was small, and its average phase relative to the LFP varied among experiments, as expected from the very sparse synaptic connectivity among pyramidal neurons in CA1 (Deuchars & Thomson, 1996). Gamma clamp imposed a large phasic inward current (**Fig. 5b**). Subtracting the vector representing the baseline phasic inward current yielded a vector representing the net excitatory current imposed by the gamma clamp (ΔE). This lagged behind the LED modulation, reflecting in part the opsin activation and deactivation kinetics (**Fig. 5c**, and arrows in **Fig. 5b**, right). For the example illustrated in Fig. 5 an 83° phase advance of the LED over the LFP resulted in ΔE with mean phase of 247°, where the LFP trough is defined as 0°. This yielded an increase in frequency and decrease in power of the gamma oscillation.

Comparing across different clamp regimes reveals how gamma frequency and power change in relation to the phasic excitation experienced by principal cells (**Fig. 6a, b**). An increase in gamma frequency was achieved when the average excitatory current phase occurred during the down-stroke of the LFP (~180° to 360°), whilst a decrease in frequency was achieved when excitation was applied during the upstroke (~0° to 180°). An increase in power, on the other hand, was achieved with excitation around the trough (~270° to 90°), and a decrease in power occurred with excitation around the peak (~90° to 270°). Given that, under baseline conditions, pyramidal neurons fire maximally near to the trough of the LFP (0°), these data imply that the increase in frequency occurs because they are brought to firing threshold earlier (see also **Fig. 4b, c**). An increase in power, on the other hand, occurs because pyramidal neurons are synchronized by adding a depolarization when they are most likely to fire (see also **Fig. 4a, c**).

Gamma clamp affects inhibitory currents

Finally, we asked how inhibitory currents in a subset of pyramidal neurons are altered by the closed-loop optogenetic manipulation, by voltage-clamping them around the glutamate reversal potential (0 mV). The mean phase and amplitude of outward inhibitory currents were calculated in a similar way, by subtracting the minimal current from the circular average of the outward $GABA_A$ receptor-mediated current (**Fig. 7**). In contrast to excitatory currents, phasic inhibitory currents under baseline conditions were large, consistent with the major role of feedback interneurons in gamma (**Fig. 7a, b**). Changes in inhibitory currents (ΔI) were

relatively smaller than for excitatory currents and were dominated by effects on the power of the oscillation. Thus, for a +83° LED-LFP phase advance, which led to a decrease in gamma power and increase in frequency (same cell as in Fig. 5), there was little change in the average phase of the inhibitory current, although it was decreased (**Fig. 7c**). Aligning the average currents by the LFP across different trials whilst the cell was held at -70 mV or 0 mV, and during unclamped and clamped periods, yielded an insight into the relationship between excitatory and inhibitory conductances during the oscillatory cycle (**Fig. 7d**). For the example shown in Fig. 5 and Fig. 7a-c, the effective cycle changed from one dominated by phasic inhibition to one with similar relative amplitudes of phasic inhibition and excitation, with excitation leading inhibition in both cases (**Fig. 7d**, left). In contrast, for a 133° LED-LFP phase delay, which led to a decrease in frequency and increase in power, the inhibitory current increased (**Fig. 7d, right**). Similar results were obtained in 8 cells.

Discussion

The present study shows that closed-loop optogenetic manipulation of principal cells allows predictable, bidirectional and dissociable changes in the power and frequency of gamma oscillations. We observed a broad consistency between the frequency manipulation achieved with closed loop optogenetic feedback and that predicted from the phase response behaviour previously observed with intermittent optogenetic stimuli (Akam et al., 2012). Optogenetically and pharmacologically induced gamma also exhibited similar dynamical properties in that study, implying that the principles uncovered in the present work are not specific to the way gamma oscillations were elicited.

Previous studies have stressed the importance of fast-spiking parvalbumin-positive (PV+) interneurons in gamma (Cardin et al., 2009; Sohal et al., 2009) (but see (Veit et al., 2017)). PV+ basket cells tend to fire with very little phase dispersion, close to one-to-one with each cycle of the oscillation *in vitro* (Bartos et al., 2007; Gulyás et al., 2010). Our attempts to achieve gamma clamp by targeting interneurons rather than pyramidal cells have thus far been unsuccessful because their out of phase recruitment powerfully suppresses the oscillation (data not shown). The weaker phase-locking of pyramidal than PV+ cell firing to gamma oscillations, together with their sparse firing on successive cycles of gamma (Csicsvari, Jamieson, Wise, & Buzsáki, 2003; Gulyás et al., 2010; Tukker, Fuentealba, Hartwich, Somogyi, & Klausberger, 2007), may however confer a broader dynamic range over which they can influence the phase, frequency and amplitude of the oscillation. Taken together with previous evidence that open-loop sinusoidal optogenetic stimulation of

principal cells can entrain a gamma oscillation (Akam et al., 2012), the present data underline the importance of action potential timing in principal cells in the spectral and temporal properties of hippocampal gamma, notwithstanding the evidence that the LFP itself is dominated by inhibitory currents in principal cells (Oren et al., 2010), and argue against a model where the function of principal cells is only to depolarize a population of reciprocally connected interneurons.

Closed-loop manipulations have been applied previously in the context of network oscillations, using either electrical and optogenetic stimuli delivered at specific phases of theta or gamma oscillations, in order to probe the mechanisms of long-term plasticity induction (Huerta & Lisman, 1995; Pavlides, Greenstein, Grudman, & Winson, 1988) or sharp-wave ripple generation (Stark et al., 2014), or to test the theta phase-dependence of memory encoding and retrieval (Siegle & Wilson, 2014). A similar strategy has been used to interrupt experimental thalamocortical seizures (Berényi, Belluscio, Mao, & Buzsáki, 2012). However, these studies have not aimed at modulating the amplitude or frequency of an on-going oscillation.

We have focused on gamma because a local circuit is sufficient to generate the oscillation, and we have previously shown that the phase response behaviour of hippocampal gamma is well described by a simple dynamical model (Akam et al., 2012). The circuits underlying theta and other oscillations either involve longer-range connections in the brain or are poorly defined. They are therefore less likely to be amenable to local optogenetic manipulation. This does not exclude the possibility that, for instance, theta oscillations in the hippocampus could be manipulated by closed-loop modulation of excitability in the basal forebrain.

The ability to alter the amplitude and frequency of gamma suggests a versatile tool to test the roles of gamma in information routing and other high-level brain functions, both in health and in disease states such as schizophrenia (Uhlhaas & Singer, 2010). Hitherto, most experimental manipulations of oscillations have relied on periodic stimulation, which can entrain network oscillations (Akam et al., 2012) or evoke oscillations in an otherwise asynchronous network (Cardin et al., 2009; Sohal et al., 2009). Transcranial stimulation designed to entrain oscillations in vivo can bias perception (Neuling, Rach, Wagner, Wolters, & Herrmann, 2012; Romei, Gross, & Thut, 2010; Thut, Schyns, & Gross, 2011) and bidirectionally affect performance in motor (Joundi, Jenkinson, Brittain, Aziz, & Brown, 2012) and working memory (Polanía, Nitsche, Korman, Batsikadze, & Paulus, 2012) tasks. However, external periodic stimulation is not well suited to desynchronize network activity or to suppress oscillatory dynamics. Furthermore, if periodic stimulation is used, the desired change in amplitude or frequency is achieved at the cost of imposing an externally

347 determined phase on the oscillation. This will prevent the oscillation from entraining to
348 endogenous periodic signals such as those arising from other oscillating networks or
349 periodic sensory stimuli.

350 Closed-loop stimulation, in which signals recorded from a network are used in real time to
351 bias its state, in principle provides an alternative way of manipulating network oscillations,
352 and has been used to interfere with pathological rhythms in models of Parkinson's disease
353 (Rosin et al., 2011), to suppress Parkinsonian tremor (Brittain, Probert-Smith, Aziz, & Brown,
354 2013), and in a model of thalamocortical epilepsy (Butt et al., 2005). This approach relies on
355 an artificial feedback loop which either counteracts or amplifies the endogenous feedback
356 responsible for synchronizing the network (Rosenblum & Pikovsky, 2004). Importantly,
357 optogenetics has the advantage over electrical stimulation that the modulation can be
358 distributed across a population of neurons. We have, moreover, shown that closed-loop
359 manipulation of a gamma oscillation can be achieved without a net increase or decrease in
360 the average firing rate of neurons, implying that it would not necessarily perturb information
361 represented as an average firing rate code.

362 Extrapolating from *in vitro* gamma to the brain *in situ* presents several technical challenges,
363 including the need for optical fibers to illuminate the tissue and the potential for
364 photoelectrical artifacts. Moreover, oscillations are generally less prominent because the
365 current generators from multiple oscillating and non-oscillating populations overlap,
366 complicating the evaluation of phase and frequency. Nevertheless, the present study
367 identifies some general principles to guide attempts to achieve bidirectional and dissociable
368 modulation of oscillatory frequency and power *in vivo*. This should allow a definitive test of
369 the causal role of gamma in functions such as attention modulation and information routing
370 (Sohal, 2016).

371

372 **Materials & Methods**

373 **Key resource table**

Reagent type (species) or resource	Designation	Source or reference	Identifiers	Additional information
Strain, strain background (*Mus*	Wild type, C57bl6 mice	UCL Biological		

Reagent type (species) or resource	Designation	Source or reference	Identifiers	Additional information
musculus)		Services		
Genetic reagent	Viral vector (C1V1): AAV5-CaMKIIa-C1V1(E122T/E162T)-TS-eYFP	UNC Vector Core	Serotype: 5 C1V1: AAV-CaMKIIa-C1V1(E122T/E162T)-TS-EYFP	
Other	Equipment (viral injections): Sterotaxic frame	Kopf Instruments	Model 900	
Chemical compound, drug	Salts, drugs	Sigma		
Other	Equipment (LED light source)	Cairn Instruments	OptoLED, 590 nm	
Other	Equipment (LED light source) Custom assembled LED	Thorlabs	High-power mounted LED: M590L2; Tube lens: SM1V10; Planoconvex lens: LA1951-A-N-BK7; Coupler: SM1T2; Adapter for microscope: SM1A14	
Other	Equipment (LED driver)	Thorlabs	DC2100	
Other	Equipment (Upright microscope)	Olympus	BX51WI, UMPLFLN 20X W IR	
Other	Equipment (Upright microscope)	Scientifica	SliceScope, UMPLFLN 20X W IR	
Other	Equipment (Amplifier)	Molecular Devices	Multiclamp 700B	
Other	Equipment (Data acquisition card)	National Instruments	PCI-6221	

Reagent type (species) or resource	Designation	Source or reference	Identifiers	Additional information
Other	Equipment (computing) Real-time controller	National Instruments	cRIO-9022	
Other	Equipment (computing). FPGA	Xilinx	Virtek-5	
Software, algorithm	LabVIEW	National Instruments	*LabVIEW, LabVIEW Real-Time* 2013, 2014, 2015, 2016, 2017	Custom virtual instruments
Software, algorithm	*R*	www.R-project.org	Ver. 3.3.0 for Mac	

374

All procedures followed the Animals (Scientific Procedures) Act, 1986, and were reviewed by the UCL Institute of Neurology Animal Welfare and Ethical Review Body. P21 male C57 mice were anesthetized with isoflurane and placed in a stereotaxic frame (Kopf Instruments). A suspension of AAV5-CaMKIIa-C1V1(E122T/E162T)-TS-eYFP (UNC Vector Core, titre 5 x 10^{12} IU/ml) was injected at a rate of 100 nl/min into 4 sites in both hippocampi (injection volume: 300-500 nl per site). The antero-posterior injection coordinate was taken as 2/3 of the distance from bregma to lambda. The lateral coordinates were 3.0 mm from the midline, and the ventral coordinates were 3.5, 3.0, 2.5 and 2.0 mm from the surface of the skull.

Hippocampal slices were prepared at least 4 weeks later. Animals were sacrificed by pentobarbitone overdose and underwent transcardiac perfusion with an oxygenated solution containing (in mM): 92 N-methyl-D-glucamine-Cl, 2.5 KCl, 1.25 NaH_2PO_4, 20 HEPES, 30 $NaHCO_3$, 25 glucose, 10 $MgCl_2$, 0.5 $CaCl_2$, 2 thiourea, 5 Na-ascorbate and 3 Na-pyruvate, with sucrose added to achieve an osmolality of 315 mOsm/L. Brain slices (400 µm thick) were prepared at room temperature and then incubated at 37 ºC for 12 minutes in the same solution. They were subsequently stored at room temperature, in a solution containing (in mM): 126 NaCl, 3 KCl, 1.25 NaH_2PO_4, 2 $MgSO_4$, 2 $CaCl_2$, 24 $NaHCO_3$, 10 glucose, shielded from light, before being transferred to the stage of an upright microscope (Olympus BX51WI or Scientifica SliceScope), where they were perfused on both sides with the same solution at 32° C. Expression of C1V1 in CA1 was verified by epifluorescence, and CA3 was ablated to focus on local gamma-generating mechanisms.

Epifluorescence imaging and C1V1 stimulation were achieved with LEDs (OptoLED, Cairn Instruments, or assembled from Thorlabs components using an M590L2 590 nm LED and a DC2100 high-power LED driver). The light source was coupled to the epifluorescence illuminator of the microscope, with a silver mirror in the place of a dichroic cube. Wide-field illumination was delivered via a 20x, 0.5 NA water immersion objective. The current delivered to the LED was kept in the linear input-output range, and the irradiance was <5 mW/mm^2. Light ramps typically lasting 8 s were delivered every 30 – 45 s.

LFPs were recorded in the CA1 pyramidal layer using patch pipettes filled with extracellular solution and a Multiclamp 700B amplifier (Molecular Devices), and band-pass filtered between 1 and 200 or 500 Hz. A linear LED ramp command was generated via a multifunction data acquisition card (National Instruments PCI-6221) and, together with the LFP, was digitized using a real-time controller (National Instruments cRIO-9022) with a Xilinx Virtex-5 FPGA (cRIO-9133) operating at a loop rate of 10 kHz. The ramp was multiplied by $(1 + k_1\mathrm{LFP} + k_2 d\mathrm{LFP}/dt)$, stepping through different values of k in a pseudo-random order for

successive trials. *d*LFP/*d*t was calculated as the difference between successive digitization values in the FPGA, averaged over successive 2 ms intervals to minimize high-frequency noise. The output of the FPGA/real-time controller was sent to the LED driver, and digitized in parallel with the LFP at 10 kHz on the data acquisition PC.

To study the phase relationship of action potentials and the LFP oscillation, a cell-attached recording was obtained using a second patch pipette held in voltage clamp mode, low-pass filtered at 10 kHz and digitized in parallel with the LFP and LED command signal. The phasic excitatory or inhibitory current was recorded in the same way, but using a whole-cell pipette containing (in mM): K-gluconate (145), NaCl (8), KOH-HEPES (10), EGTA (0.2), Mg-ATP (2) and Na 3 -GTP (0.3); pH 7.2; 290 mOsm. Phasic conductances (Fig. 7d) were estimated from Ohm's law, assuming a driving force of 70 mV.

Off-line analysis was performed in LabVIEW (National Instruments) and R. Time-frequency spectrograms were calculated using a Morlet wavelet transform and are displayed as heat maps. Because the gamma oscillation was non-stationary, its frequency was estimated by calculating the short-term Fourier transform and then averaging the mean instantaneous frequency for successive overlapping intervals. The power of the oscillation was estimated in the same way, by averaging the power at the mean instantaneous frequency.

Spikes were identified using threshold crossing. The instantaneous oscillation phase was estimated by passing a 200-ms segment of the LFP centered on the spike through a Hanning window, and then calculating its phase and frequency using the Extract Single Tone VI in LabVIEW.

To estimate the phase relationship between spikes or membrane currents and the gamma oscillation, we first identified successive troughs of the LFP using the WA Multiscale Peak Detection VI in LabVIEW. Gamma cycles that deviated more than 20% from the modal period were rejected. The membrane current waveform between successive troughs was then expressed as a function of instantaneous phase and averaged over all accepted cycles in the interval. The minimal (least negative) inward current recorded at -70 mV was subtracted to yield the average phasic excitatory current waveform. To estimate the phasic inhibitory current waveform, the minimal outward current was subtracted whilst holding cells at 0 mV.

Acknowledgments

We are grateful to Francis Carpenter, Flora Lee and Iris Oren for pilot experiments, and to Karl Deisseroth for sharing C1V1. This work was supported by the Wellcome Trust.

Competing interests

The authors declare no competing interests

References

Adesnik, H. (2018). Layer-specific excitation/inhibition balances during neuronal synchronization in the visual cortex. *The Journal of Physiology*. https://doi.org/10.1113/JP274986

Adesnik, H., & Scanziani, M. (2010). Lateral competition for cortical space by layer-specific horizontal circuits. *Nature*, *464*(7292), 1155–1160. https://doi.org/10.1038/nature08935

Akam, T., & Kullmann, D. M. (2010). Oscillations and filtering networks support flexible routing of information. *Neuron*, *67*(2), 308–320. https://doi.org/10.1016/j.neuron.2010.06.019

Akam, T., & Kullmann, D. M. (2014). Oscillatory multiplexing of population codes for selective communication in the mammalian brain. *Nature Reviews. Neuroscience*, *15*(2), 111–122. https://doi.org/10.1038/nrn3668

Akam, T., Oren, I., Mantoan, L., Ferenczi, E., & Kullmann, D. M. (2012). Oscillatory dynamics in the hippocampus support dentate gyrus–CA3 coupling. *Nature Neuroscience*, *15*(5), 763–768. https://doi.org/10.1038/nn.3081

Akao, A., Ogawa, Y., Jimbo, Y., Ermentrout, G. B., & Kotani, K. (2018). Relationship between the mechanisms of gamma rhythm generation and the magnitude of the macroscopic phase response function in a population of excitatory and inhibitory modified quadratic integrate-and-fire neurons. *Physical Review. E*, *97*(1–1), 012209. https://doi.org/10.1103/PhysRevE.97.012209

Bartos, M., Vida, I., Frotscher, M., Meyer, A., Monyer, H., Geiger, J. R. P., & Jonas, P. (2002). Fast synaptic inhibition promotes synchronized gamma oscillations in hippocampal interneuron networks. *Proceedings of the National Academy of Sciences of the United States of America*, *99*(20), 13222–13227. https://doi.org/10.1073/pnas.192233099

Bartos, M., Vida, I., & Jonas, P. (2007). Synaptic mechanisms of synchronized gamma oscillations in inhibitory interneuron networks. *Nature Reviews. Neuroscience*, *8*(1), 45–56. https://doi.org/10.1038/nrn2044

Berényi, A., Belluscio, M., Mao, D., & Buzsáki, G. (2012). Closed-Loop Control of Epilepsy by Transcranial Electrical Stimulation. *Science*, *337*(6095), 735–737. https://doi.org/10.1126/science.1223154

Börgers, C., & Kopell, N. (2003). Synchronization in networks of excitatory and inhibitory neurons with sparse, random connectivity. *Neural Computation*, *15*(3), 509–538. https://doi.org/10.1162/089976603321192059

Bosman, C. A., Schoffelen, J.-M., Brunet, N., Oostenveld, R., Bastos, A. M., Womelsdorf, T., … Fries, P. (2012). Attentional stimulus selection through selective synchronization between monkey visual areas. *Neuron*, *75*(5), 875–888. https://doi.org/10.1016/j.neuron.2012.06.037

Brittain, J.-S., Probert-Smith, P., Aziz, T. Z., & Brown, P. (2013). Tremor suppression by rhythmic transcranial current stimulation. *Current Biology: CB*, *23*(5), 436–440. https://doi.org/10.1016/j.cub.2013.01.068

Butler, J. L., Mendonça, P. R. F., Robinson, H. P. C., & Paulsen, O. (2016). Intrinsic Cornu Ammonis Area 1 Theta-Nested Gamma Oscillations Induced by Optogenetic Theta Frequency Stimulation. *The Journal of Neuroscience: The Official Journal of the Society for Neuroscience*, *36*(15), 4155–4169. https://doi.org/10.1523/JNEUROSCI.3150-15.2016

Butt, S. J. B., Fuccillo, M., Nery, S., Noctor, S., Kriegstein, A., Corbin, J. G., & Fishell, G. (2005). The temporal and spatial origins of cortical interneurons predict their physiological subtype. *Neuron*, *48*(4), 591–604. https://doi.org/10.1016/j.neuron.2005.09.034

Buzsáki, G., & Schomburg, E. W. (2015). What does gamma coherence tell us about inter-regional neural communication? *Nature Neuroscience*, *18*(4), 484–489. https://doi.org/10.1038/nn.3952

Buzsáki, G., & Wang, X.-J. (2012). Mechanisms of gamma oscillations. *Annual Review of Neuroscience*, *35*, 203–225. https://doi.org/10.1146/annurev-neuro-062111-150444

Cardin, J. A., Carlén, M., Meletis, K., Knoblich, U., Zhang, F., Deisseroth, K., … Moore, C. I. (2009). Driving fast-spiking cells induces gamma rhythm and controls sensory responses. *Nature*, *459*(7247), 663–667. https://doi.org/10.1038/nature08002

Cole, S. R., & Voytek, B. (2017). Brain Oscillations and the Importance of Waveform Shape. *Trends in Cognitive Sciences*, *21*(2), 137–149. https://doi.org/10.1016/j.tics.2016.12.008

Colgin, L. L., Denninger, T., Fyhn, M., Hafting, T., Bonnevie, T., Jensen, O., … Moser, E. I. (2009). Frequency of gamma oscillations routes flow of information in the hippocampus. *Nature*, *462*(7271), 353–357. https://doi.org/10.1038/nature08573

Csicsvari, J., Jamieson, B., Wise, K. D., & Buzsáki, G. (2003). Mechanisms of gamma oscillations in the hippocampus of the behaving rat. *Neuron*, *37*(2), 311–322.

Deuchars, J., & Thomson, A. M. (1996). CA1 pyramid-pyramid connections in rat hippocampus in vitro: dual intracellular recordings with biocytin filling. *Neuroscience*, *74*(4), 1009–1018.

Fisahn, A., Contractor, A., Traub, R. D., Buhl, E. H., Heinemann, S. F., & McBain, C. J. (2004). Distinct roles for the kainate receptor subunits GluR5 and GluR6 in kainate-induced hippocampal gamma oscillations. *The Journal of Neuroscience: The Official Journal of the Society for Neuroscience*, *24*(43), 9658–9668. https://doi.org/10.1523/JNEUROSCI.2973-04.2004

Fisahn, A., Pike, F. G., Buhl, E. H., & Paulsen, O. (1998). Cholinergic induction of network oscillations at 40 Hz in the hippocampus in vitro. *Nature*, *394*(6689), 186–189. https://doi.org/10.1038/28179

Fries, P. (2005). A mechanism for cognitive dynamics: neuronal communication through

519 neuronal coherence. *Trends in Cognitive Sciences*, *9*(10), 474–480.
520 https://doi.org/10.1016/j.tics.2005.08.011

521 Fries, P. (2015). Rhythms for Cognition: Communication through Coherence. *Neuron*, *88*(1),
522 220–235. https://doi.org/10.1016/j.neuron.2015.09.034

523 Grosenick, L., Marshel, J. H., & Deisseroth, K. (2015). Closed-loop and activity-guided
524 optogenetic control. *Neuron*, *86*(1), 106–139. https://doi.org/10.1016/j.neuron.2015.03.034

525 Grothe, I., Neitzel, S. D., Mandon, S., & Kreiter, A. K. (2012). Switching neuronal inputs by
526 differential modulations of gamma-band phase-coherence. *The Journal of Neuroscience:*
527 *The Official Journal of the Society for Neuroscience*, *32*(46), 16172–16180.
528 https://doi.org/10.1523/JNEUROSCI.0890-12.2012

529 Gulyás, A. I., Szabó, G. G., Ulbert, I., Holderith, N., Monyer, H., Erdélyi, F., … Hájos, N.
530 (2010). Parvalbumin-containing fast-spiking basket cells generate the field potential
531 oscillations induced by cholinergic receptor activation in the hippocampus. *The Journal of*
532 *Neuroscience: The Official Journal of the Society for Neuroscience*, *30*(45), 15134–15145.
533 https://doi.org/10.1523/JNEUROSCI.4104-10.2010

534 Hájos, N., Pálhalmi, J., Mann, E. O., Németh, B., Paulsen, O., & Freund, T. F. (2004). Spike
535 Timing of Distinct Types of GABAergic Interneuron during Hippocampal Gamma Oscillations
536 In Vitro. *The Journal of Neuroscience*, *24*(41), 9127–9137.
537 https://doi.org/10.1523/JNEUROSCI.2113-04.2004

538 Huerta, P. T., & Lisman, J. E. (1995). Bidirectional synaptic plasticity induced by a single
539 burst during cholinergic theta oscillation in CA1 in vitro. *Neuron*, *15*(5), 1053–1063.

540 Joundi, R. A., Jenkinson, N., Brittain, J.-S., Aziz, T. Z., & Brown, P. (2012). Driving
541 Oscillatory Activity in the Human Cortex Enhances Motor Performance. *Current Biology*,
542 *22*(5), 403–407. https://doi.org/10.1016/j.cub.2012.01.024

543 Kirst, C., Timme, M., & Battaglia, D. (2016). Dynamic information routing in complex
544 networks. *Nature Communications*, *7*, 11061. https://doi.org/10.1038/ncomms11061

545 Kotani, K., Yamaguchi, I., Yoshida, L., Jimbo, Y., & Ermentrout, G. B. (2014). Population
546 dynamics of the modified theta model: macroscopic phase reduction and bifurcation analysis
547 link microscopic neuronal interactions to macroscopic gamma oscillation. *Journal of the*
548 *Royal Society, Interface*, *11*(95), 20140058. https://doi.org/10.1098/rsif.2014.0058

549 Krook-Magnuson, E., Armstrong, C., Oijala, M., & Soltesz, I. (2013). On-demand optogenetic
550 control of spontaneous seizures in temporal lobe epilepsy. *Nature Communications*, *4*, 1376.
551 https://doi.org/10.1038/ncomms2376

552 Lisman, J. (2010). Working memory: the importance of theta and gamma oscillations.
553 *Current Biology: CB*, *20*(11), R490-492. https://doi.org/10.1016/j.cub.2010.04.011

554 Lu, Y., Truccolo, W., Wagner, F. B., Vargas-Irwin, C. E., Ozden, I., Zimmermann, J. B., …
555 Nurmikko, A. V. (2015). Optogenetically induced spatiotemporal gamma oscillations and
556 neuronal spiking activity in primate motor cortex. *Journal of Neurophysiology*, *113*(10),
557 3574–3587. https://doi.org/10.1152/jn.00792.2014

558 Mann, E. O., Radcliffe, C. A., & Paulsen, O. (2005). Hippocampal gamma-frequency

559 oscillations: from interneurones to pyramidal cells, and back. *The Journal of Physiology*,
560 *562*(1), 55–63. https://doi.org/10.1113/jphysiol.2004.078758

561 Neuling, T., Rach, S., Wagner, S., Wolters, C. H., & Herrmann, C. S. (2012). Good
562 vibrations: oscillatory phase shapes perception. *NeuroImage*, *63*(2), 771–778.
563 https://doi.org/10.1016/j.neuroimage.2012.07.024

564 Newman, J. P., Fong, M., Millard, D. C., Whitmire, C. J., Stanley, G. B., & Potter, S. M.
565 (2015). Optogenetic feedback control of neural activity. *ELife*, *4*, e07192.
566 https://doi.org/10.7554/eLife.07192

567 Ni, J., Wunderle, T., Lewis, C. M., Desimone, R., Diester, I., & Fries, P. (2016). Gamma-
568 Rhythmic Gain Modulation. *Neuron*, *92*(1), 240–251.
569 https://doi.org/10.1016/j.neuron.2016.09.003

570 Oren, I., Hájos, N., & Paulsen, O. (2010). Identification of the current generator underlying
571 cholinergically induced gamma frequency field potential oscillations in the hippocampal CA3
572 region. *The Journal of Physiology*, *588*(5), 785–797.
573 https://doi.org/10.1113/jphysiol.2009.180851

574 Pastoll, H., Solanka, L., van Rossum, M. C. W., & Nolan, M. F. (2013). Feedback inhibition
575 enables θ-nested γ oscillations and grid firing fields. *Neuron*, *77*(1), 141–154.
576 https://doi.org/10.1016/j.neuron.2012.11.032

577 Pavlides, C., Greenstein, Y. J., Grudman, M., & Winson, J. (1988). Long-term potentiation in
578 the dentate gyrus is induced preferentially on the positive phase of theta-rhythm. *Brain*
579 *Research*, *439*(1–2), 383–387.

580 Paz, J. T., Davidson, T. J., Frechette, E. S., Delord, B., Parada, I., Peng, K., … Huguenard,
581 J. R. (2013). Closed-loop optogenetic control of thalamus as a tool for interrupting seizures
582 after cortical injury. *Nature Neuroscience*, *16*(1), 64–70. https://doi.org/10.1038/nn.3269

583 Polanía, R., Nitsche, M. A., Korman, C., Batsikadze, G., & Paulus, W. (2012). The
584 importance of timing in segregated theta phase-coupling for cognitive performance. *Current*
585 *Biology: CB*, *22*(14), 1314–1318. https://doi.org/10.1016/j.cub.2012.05.021

586 Rodriguez, E., George, N., Lachaux, J.-P., Martinerie, J., Renault, B., & Varela, F. J. (1999).
587 Perception's shadow: long-distance synchronization of human brain activity. *Nature*,
588 *397*(6718), 430–433. https://doi.org/10.1038/17120

589 Romei, V., Gross, J., & Thut, G. (2010). On the role of prestimulus alpha rhythms over
590 occipito-parietal areas in visual input regulation: correlation or causation? *The Journal of*
591 *Neuroscience: The Official Journal of the Society for Neuroscience*, *30*(25), 8692–8697.
592 https://doi.org/10.1523/JNEUROSCI.0160-10.2010

593 Rosenblum, M. G., & Pikovsky, A. S. (2004). Controlling synchronization in an ensemble of
594 globally coupled oscillators. *Physical Review Letters*, *92*(11), 114102.

595 Rosin, B., Slovik, M., Mitelman, R., Rivlin-Etzion, M., Haber, S. N., Israel, Z., … Bergman, H.
596 (2011). Closed-Loop Deep Brain Stimulation Is Superior in Ameliorating Parkinsonism.
597 *Neuron*, *72*(2), 370–384. https://doi.org/10.1016/j.neuron.2011.08.023

598 Salinas, E., & Sejnowski, T. J. (2001). Correlated neuronal activity and the flow of neural

599 information. *Nature Reviews. Neuroscience*, *2*(8), 539–550.
600 https://doi.org/10.1038/35086012

601 Schnitzler, A., & Gross, J. (2005). Normal and pathological oscillatory communication in the
602 brain. *Nat Rev Neurosci*, *6*(4), 285–296. https://doi.org/10.1038/nrn1650

603 Siegle, J. H., & Wilson, M. A. (2014). Enhancement of encoding and retrieval functions
604 through theta phase-specific manipulation of hippocampus. *ELife*, *3*, e03061.
605 https://doi.org/10.7554/eLife.03061

606 Sohal, V. S. (2016). How Close Are We to Understanding What (if Anything) γ Oscillations
607 Do in Cortical Circuits? *The Journal of Neuroscience: The Official Journal of the Society for*
608 *Neuroscience*, *36*(41), 10489–10495. https://doi.org/10.1523/JNEUROSCI.0990-16.2016

609 Sohal, V. S., Zhang, F., Yizhar, O., & Deisseroth, K. (2009). Parvalbumin neurons and
610 gamma rhythms enhance cortical circuit performance. *Nature*, *459*(7247), 698–702.
611 https://doi.org/10.1038/nature07991

612 Stark, E., Roux, L., Eichler, R., Senzai, Y., Royer, S., & Buzsáki, G. (2014). Pyramidal cell-
613 interneuron interactions underlie hippocampal ripple oscillations. *Neuron*, *83*(2), 467–480.
614 https://doi.org/10.1016/j.neuron.2014.06.023

615 Thut, G., Schyns, P. G., & Gross, J. (2011). Entrainment of perceptually relevant brain
616 oscillations by non-invasive rhythmic stimulation of the human brain. *Frontiers in*
617 *Psychology*, *2*, 170. https://doi.org/10.3389/fpsyg.2011.00170

618 Tiesinga, P., & Sejnowski, T. J. (2009). Cortical Enlightenment: Are Attentional Gamma
619 Oscillations Driven by ING or PING? *Neuron*, *63*(6), 727–732.
620 https://doi.org/10.1016/j.neuron.2009.09.009

621 Tukker, J. J., Fuentealba, P., Hartwich, K., Somogyi, P., & Klausberger, T. (2007). Cell type-
622 specific tuning of hippocampal interneuron firing during gamma oscillations in vivo. *The*
623 *Journal of Neuroscience: The Official Journal of the Society for Neuroscience*, *27*(31), 8184–
624 8189. https://doi.org/10.1523/JNEUROSCI.1685-07.2007

625 Uhlhaas, P. J., & Singer, W. (2010). Abnormal neural oscillations and synchrony in
626 schizophrenia. *Nature Reviews. Neuroscience*, *11*(2), 100–113.
627 https://doi.org/10.1038/nrn2774

628 Varela, F., Lachaux, J. P., Rodriguez, E., & Martinerie, J. (2001). The brainweb: phase
629 synchronization and large-scale integration. *Nature Reviews. Neuroscience*, *2*(4), 229–239.
630 https://doi.org/10.1038/35067550

631 Veit, J., Hakim, R., Jadi, M. P., Sejnowski, T. J., & Adesnik, H. (2017). Cortical gamma band
632 synchronization through somatostatin interneurons. *Nature Neuroscience*, *20*(7), 951–959.
633 https://doi.org/10.1038/nn.4562

634 Wang, X. J., & Buzsáki, G. (1996). Gamma oscillation by synaptic inhibition in a
635 hippocampal interneuronal network model. *The Journal of Neuroscience: The Official*
636 *Journal of the Society for Neuroscience*, *16*(20), 6402–6413.

637 Whittington, M. A., Traub, R. D., & Jefferys, J. G. (1995). Synchronized oscillations in
638 interneuron networks driven by metabotropic glutamate receptor activation. *Nature*,

639 *373*(6515), 612–615. https://doi.org/10.1038/373612a0

640 Wilson, H. R., & Cowan, J. D. (1972). Excitatory and inhibitory interactions in localized
641 populations of model neurons. *Biophysical Journal*, *12*(1), 1–24.
642 https://doi.org/10.1016/S0006-3495(72)86068-5

643 Witt, A., Palmigiano, A., Neef, A., El Hady, A., Wolf, F., & Battaglia, D. (2013). Controlling
644 the oscillation phase through precisely timed closed-loop optogenetic stimulation: a
645 computational study. *Frontiers in Neural Circuits*, *7*. https://doi.org/10.3389/fncir.2013.00049

646 Yizhar, O., Fenno, L. E., Prigge, M., Schneider, F., Davidson, T. J., O'Shea, D. J., …
647 Deisseroth, K. (2011). Neocortical excitation/inhibition balance in information processing and
648 social dysfunction. *Nature*, *477*(7363), 171–178. https://doi.org/10.1038/nature10360

649 Zar, J. H. (2009). *Biostatistical Analysis 5th By Jerrold H. Zar* (5th edition). Noida: PIE.

650

651

Figure Legends

Fig. 1. Closed-loop modulation of gamma oscillation

(a) Experimental design. The LFP in CA1 was used to modulate a ramp command generated by the PC via a field-programmable gate array (FPGA). The modulated ramp voltage command was then passed to the light-emitting diode (LED) driver, which implemented a threshold-linear voltage-to-current conversion.
(b) Unmodulated oscillation recorded in CA1 induced by a linear ramp LED driver command. Black trace: LFP with an expanded section showing the characteristic shape of the gamma oscillation (inset). Red trace: LED ramp command. Bottom: LFP Morlet wavelet spectrogram.
(c) Closed-loop oscillation clamp applied between 6 and 8 s, obtained by multiplying the ramp command by $(1 + k_1\mathrm{LFP} + k_2 d\mathrm{LFP}/dt)$, with dLFP/dt averaged over 2 ms intervals. For this example, $k_1 = 0$ mV^{-1}, $k_2 = 25$ ms mV^{-1}. The oscillation amplitude was reduced by approximately 60% (insets), with no net change in frequency.

Fig. 2. Gamma clamp allows bidirectional modulation of frequency and power

(a) In-phase modulation led to an increase in gamma power and frequency. Top: 200 ms-long segments of the LFP before, during and after closed-loop modulation of the LED driver. Middle: spectrogram. Bottom, left: two cycles of the average oscillation before and during the oscillation clamp. The average LED command (red trace, arbitrary scale) is shown superimposed on the clamped oscillation. Right: power spectral density before (blue), during (red) and after (grey) clamp. The polar plot shows the phase relationship between the LED command and the LFP.
(b) Anti-phase modulation led to decreases in both frequency and power.
(c) An increase in oscillation frequency, together with a decrease in power, was obtained with ~90° phase-advance of the LED driver command over the LFP.
(d) A decrease in frequency, together with an increase in power, was obtained when the LED modulation was delayed relative to the LFP by ~145°.
Scale bars apply to all panels.

Fig. 3. Dissociable modulation of oscillation frequency and power

(a) Dependence of frequency change on the phase relationship between the LED modulation and the LFP (positive values indicate LED phase advance relative to LFP). Changes in frequency are plotted as $F_{clamped}/F_{unclamped}$, where the unclamped frequency was averaged from the gamma oscillation for 1 s before and 1 s after the gamma clamp was applied. Data are shown as mean ± SEM (n = 19 experiments). A positive phase difference indicates that the modulation was phase-advanced relative to the LFP.
(b) Dependence of power change on the phase difference plotted as in (A).
(c) Change in frequency plotted against change in power for different LED – LFP phase differences (colour code at right).
(d) Average LFP and phase response (PRC) curve from (Akam et al., 2012) (left). The circular cross-correlogram at right yields a prediction of the effect of

a continuous modulation on the oscillation phase, and therefore on its frequency, in rough agreement with the observed relationship in (**a**).

Fig. 4. Gamma clamp alters the synchrony and phase, rather than rate, of principal cell firing

(a) Example closed loop modulation increasing gamma power. Top: red trace showing ramp command. Middle: spectrogram. Bottom: sample traces before (Unclamped) and during (Clamped) closed-loop modulation, showing the LFP and the cell-attached recording with identified spikes highlighted. LFP troughs are indicated by open circles. Six representative LFP traces, aligned by spike time, are shown at right. The polar plot indicates the distribution of spike phase for unclamped (black) and clamped (red) periods (averaged from 32 trials). The circular histograms sample spikes in 30° bins, and show a decrease in dispersion of spike phase during gamma clamp (LFP trough = 0°).

(b) Example closed loop modulation increasing gamma frequency, plotted as for (A). The polar plot indicates phase advance of spiking.

(c) Left: Bidirectional changes in power were associated with corresponding changes in the vector length (*R*) obtained by averaging all spike phases. This is consistent with a decrease in phase dispersion observed with an increase in power, and conversely, an increase in phase scatter with a decrease in power. Changes in power however did not affect the average rate of spiking, when compared with trials when gamma clamp was not applied (middle). Right: increased gamma frequency was associated with a significant phase advance of spiking. *: $p<0.05$; ***: $p<0.001$. Numbers of experiments are indicated in the bars.

Fig. 5. Gamma clamp imposes a phasic excitatory current to pyramidal neurons

(a) Top: sample LFP (black) and simultaneously recorded holding current in one pyramidal neuron held at –70 mV (blue) before, during and after feedback modulation increasing oscillatory frequency. Bottom: spectrogram.

(b) Two cycles of the average LFP waveform and membrane current without (Unclamped) and with gamma clamp (Clamped). The average phase-advanced LED command during feedback modulation is shown superimposed (red). The minimum (least negative) inward current was subtracted (dashed lines) to estimate the phasic excitation. The red arrows indicate the temporal relationship between the peak LED driver command and the maximal excitatory current. Bottom: polar plots indicating the cycle-average of the excitatory current during unclamped (left) and clamped (right) periods of the trial shown in (a). The vectors indicate the average phases of the currents.

(c) Left: difference vector obtained from the vectors in (b), representing the net phasic excitatory current imposed by gamma clamp. Right: phase difference between LED and LFP for the same experiment.

Fig. 6. Excitatory current phase determines changes in frequency and power

(a) Change in gamma frequency and power, plotted against the phase of the net excitatory current (ΔE) calculated as in Fig. 5. Confidence intervals are SEM (n = 13).

(b) $F_{clamped}/F_{unclamped}$ plotted against $P_{clamped}/P_{unclamped}$ for different excitatory current phases, indicated by the colour code below, aligned with the average LFP waveform. Pyramidal neurons spike around the trough of the LFP (0°).

Fig. 7. Gamma clamp afffects phasic inhibitory currents in pyramidal neurons

(a) Top: sample LFP (black) and simultaneously recorded holding current in one pyramidal neuron held at 0 mV (blue) before, during and after feedback modulation increasing oscillatory frequency. Bottom: spectrogram. Same cell as in Fig. 5.

(b) Two cycles of the average LFP waveform and membrane current without (Unclamped) and with gamma clamp (Clamped). The average phase-advanced LED command during feedback modulation is shown superimposed (red). The minimum (least positive) outward current was subtracted (dashed lines) to estimate the phasic inhibition.

(c) Polar plots indicating the cycle-average of the inhibitory current during unclamped (left) and clamped (right) periods of the trial shown in (a). The vectors indicate the average phases of the currents.

(d) Left: phasic inhibition (vertical scale) plotted against phasic excitation (horizontal scale) estimated by aligning cycle-average membrane conductances by the LFP without (black) and with (red) oscillation clamp with +83° LED-LFP phase advance. Same cell and clamp regime as shown in (a-c). Right: representative example of excitatory and inhibitory conductances obtained with 133° LED-LFP phase delay. Same cell but different clamp regime. The cycles are arbitrarily anchored to the trough of the LFP (*). The arrows indicate the direction of the excursion.

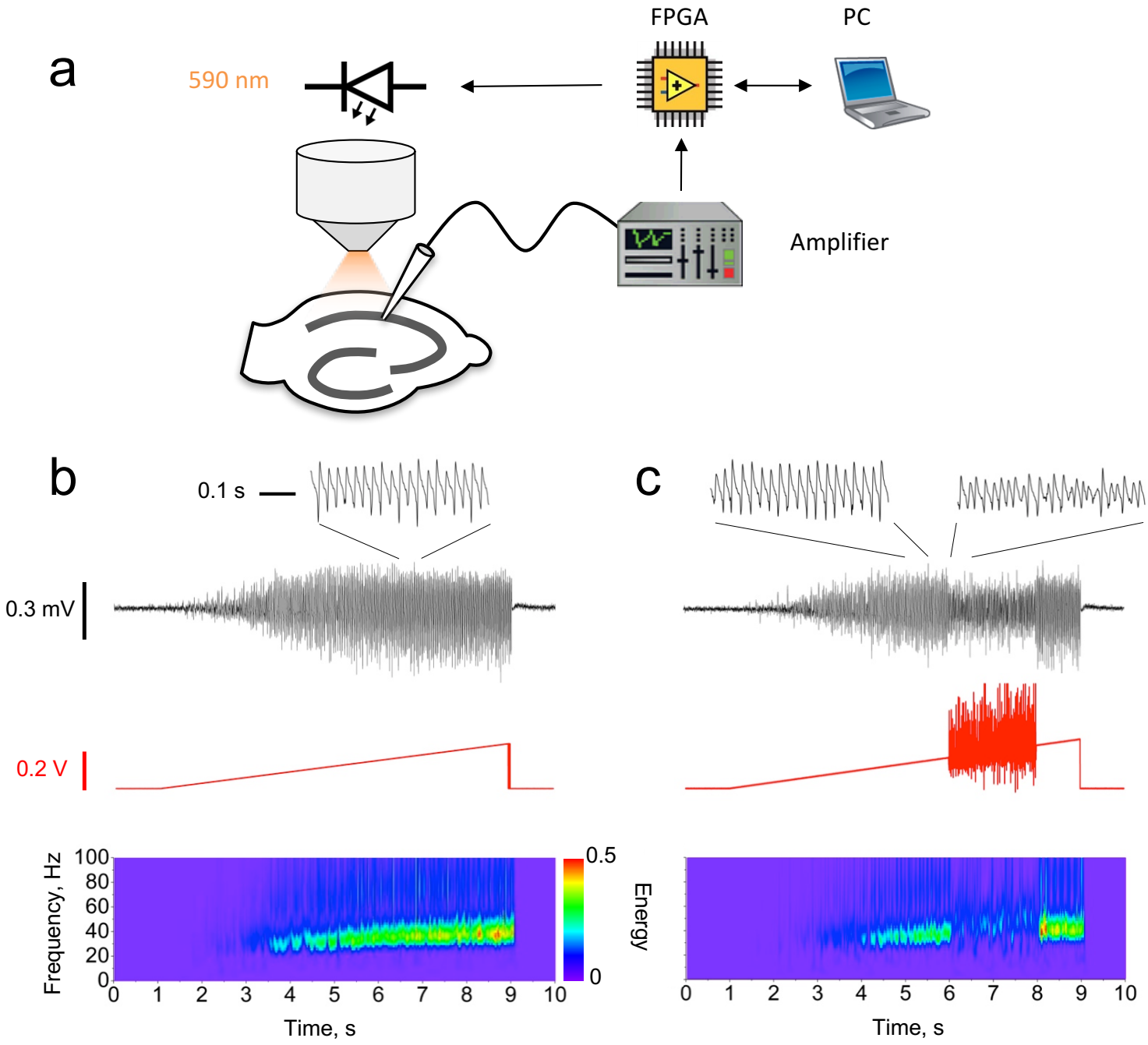
a
590 nm
FPGA
PC
Amplifier
b
0.1 s
0.3 mV
0.2 V
Frequency, Hz
100
80
60
40
20
0
0 1 2 3 4 5 6 7 8 9 10
Time, s
0.5
0
c
Energy
0 1 2 3 4 5 6 7 8 9 10
Time, s

Fig. 1

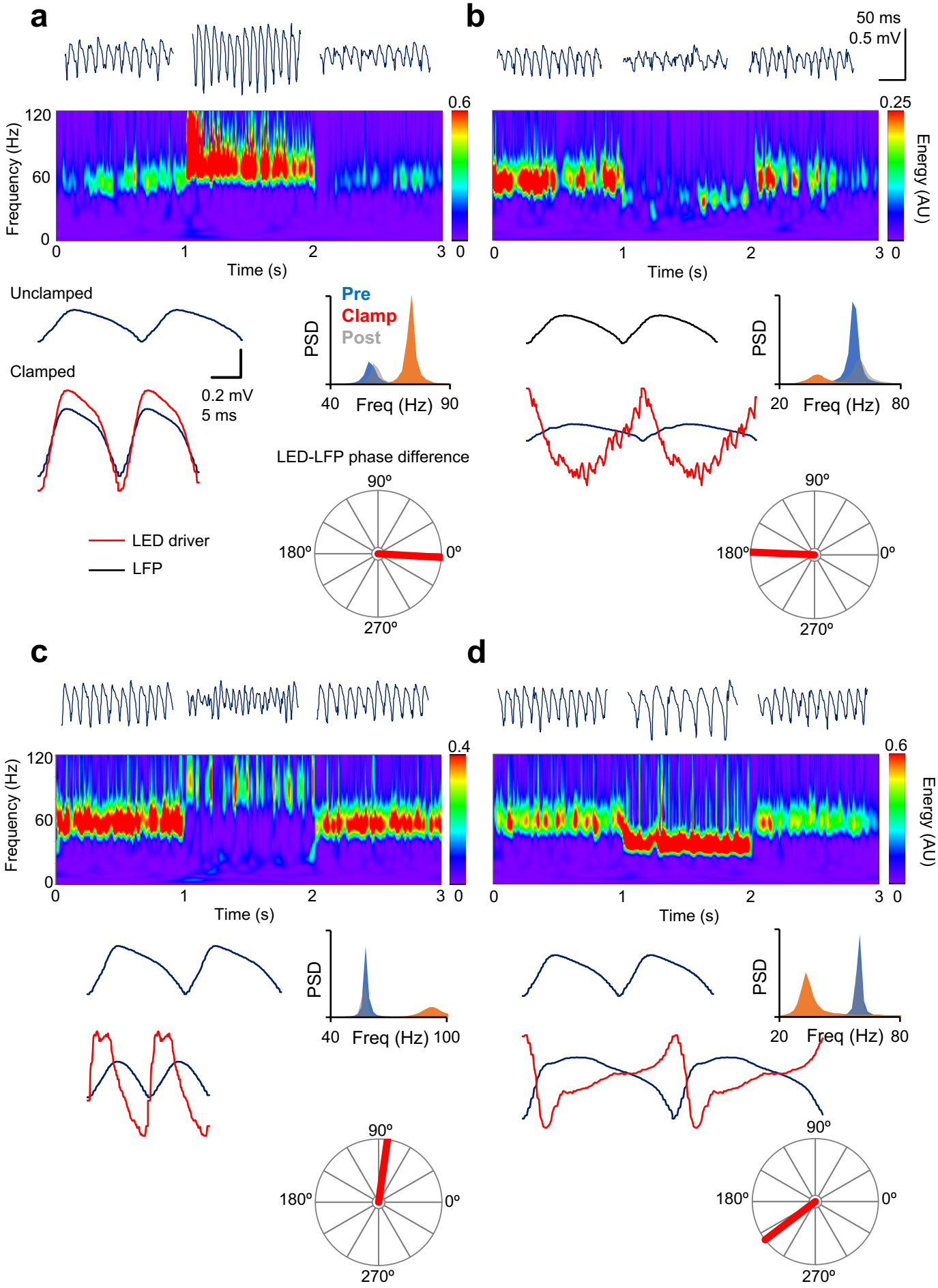
a
b
50 ms
0.5 mV
Frequency (Hz)
120
60
0
0.6
0.25
Energy (AU)
Time (s)
Unclamped
Clamped
0.2 mV
5 ms
LED driver
LFP
Pre
Clamp
Post
PSD
40
Freq (Hz)
90
20
80
LED-LFP phase difference
90°
180°
0°
270°
c
d
0.4
100

Fig. 2

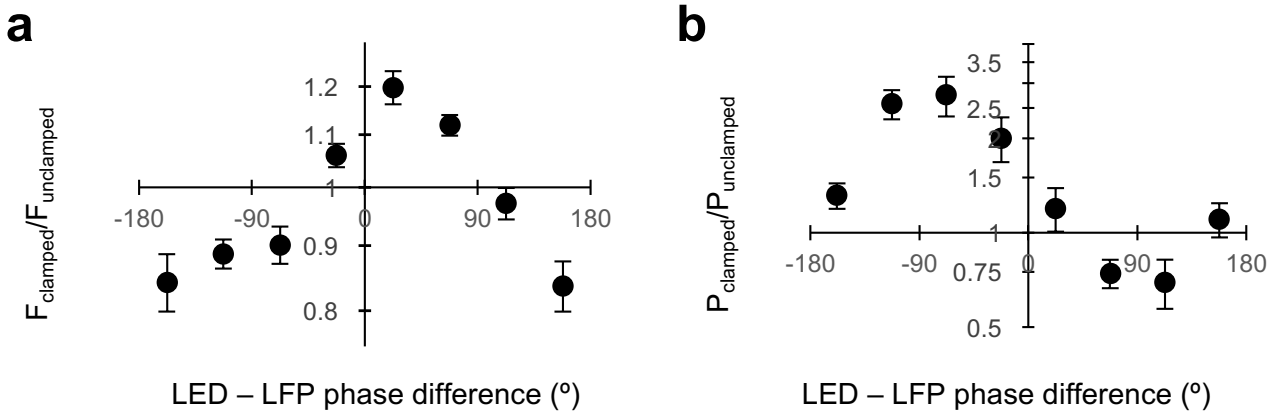
a
b
$F_{clamped}/F_{unclamped}$
$P_{clamped}/P_{unclamped}$
LED – LFP phase difference (°)
LED – LFP phase difference (°)

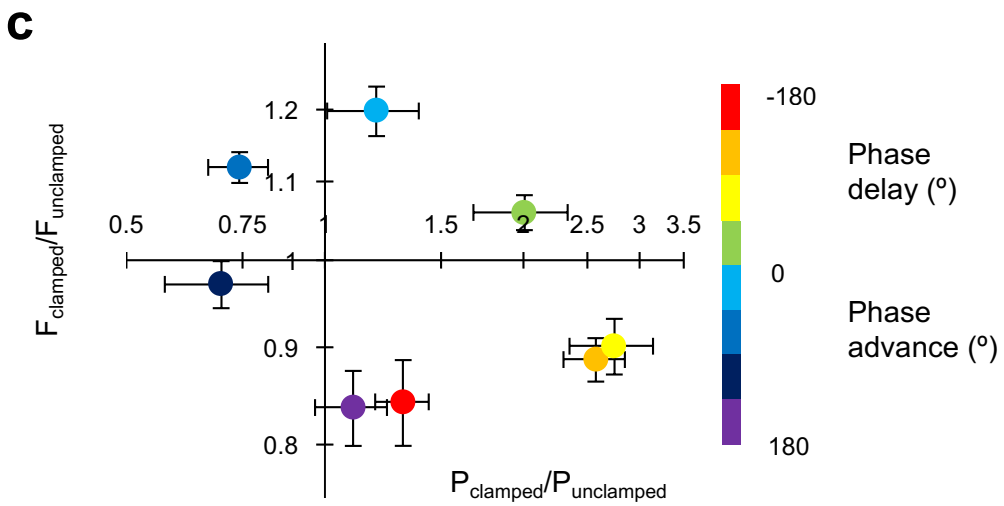
c
$F_{clamped}/F_{unclamped}$
$P_{clamped}/P_{unclamped}$
Phase delay (°)
Phase advance (°)

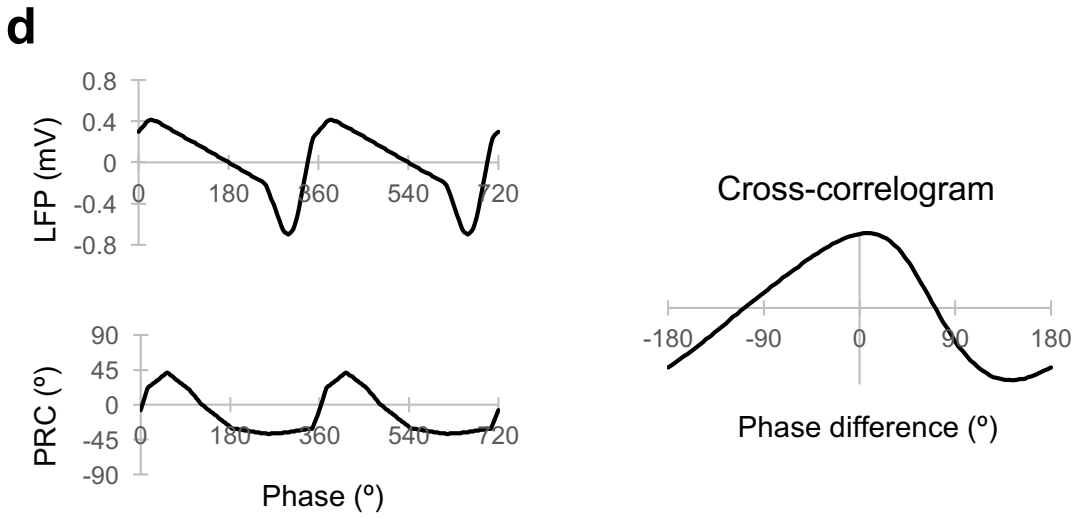
d
LFP (mV)
PRC (°)
Phase (°)
Cross-correlogram
Phase difference (°)

Fig. 3

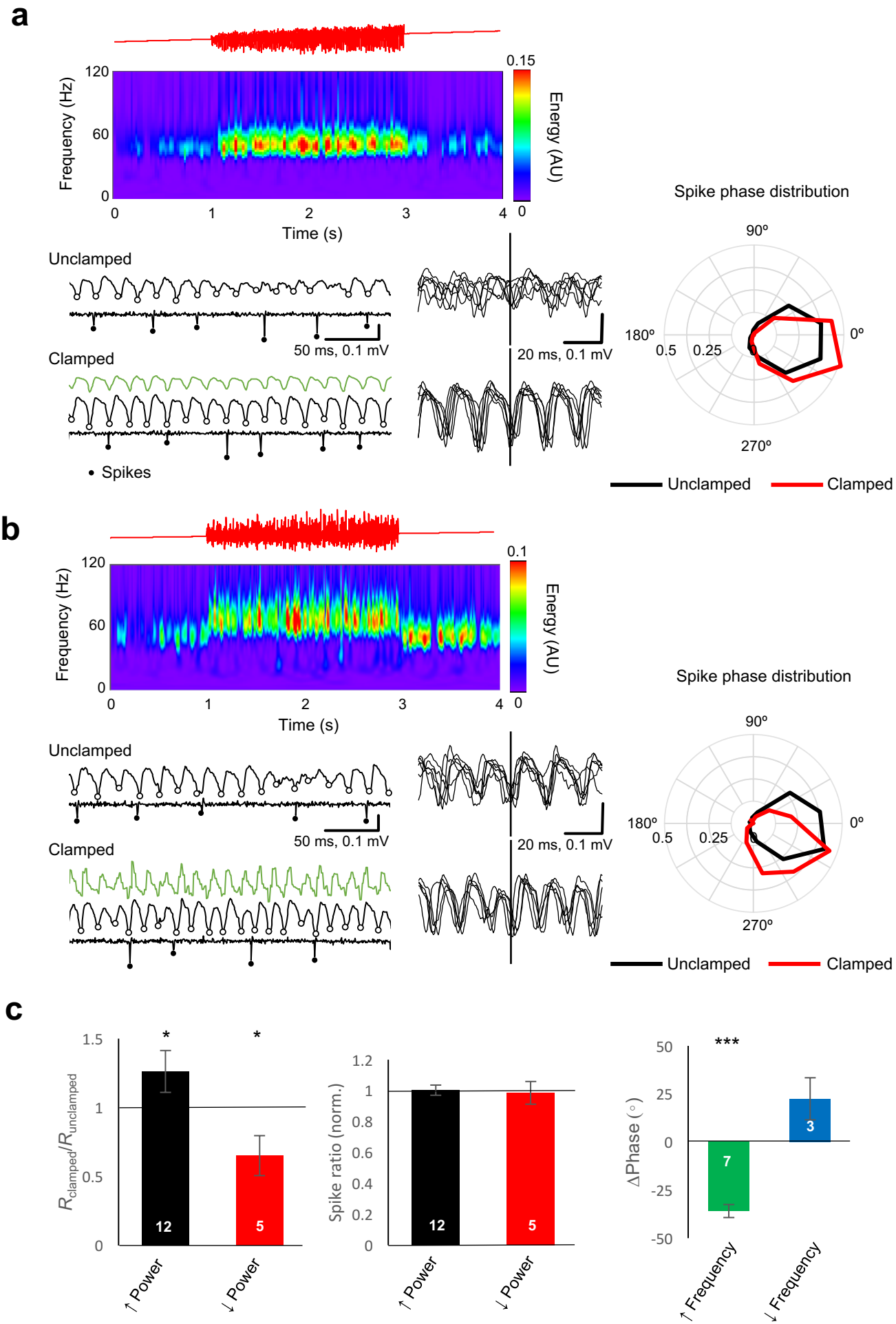
a
Frequency (Hz)
120
60
0
0
1
2
3
4
Time (s)
0.15
0
Energy (AU)
Unclamped
50 ms, 0.1 mV
20 ms, 0.1 mV
Clamped
Spikes
Spike phase distribution
90°
180°
0°
270°
0.5
0.25
Unclamped
Clamped
b
Frequency (Hz)
120
60
0
0
1
2
3
4
Time (s)
0.1
0
Energy (AU)
Unclamped
50 ms, 0.1 mV
20 ms, 0.1 mV
Clamped
Spike phase distribution
90°
180°
0°
270°
0.5
0.25
Unclamped
Clamped
c
$R_{clamped}/R_{unclamped}$
1.5
1
0.5
0
*
*
12
5
↑ Power
↓ Power
Spike ratio (norm.)
1.2
1
0.8
0.6
0.4
0.2
0
12
5
↑ Power
↓ Power
ΔPhase (°)
50
25
0
-25
-50
***
7
3
↑ Frequency
↓ Frequency

Fig. 4

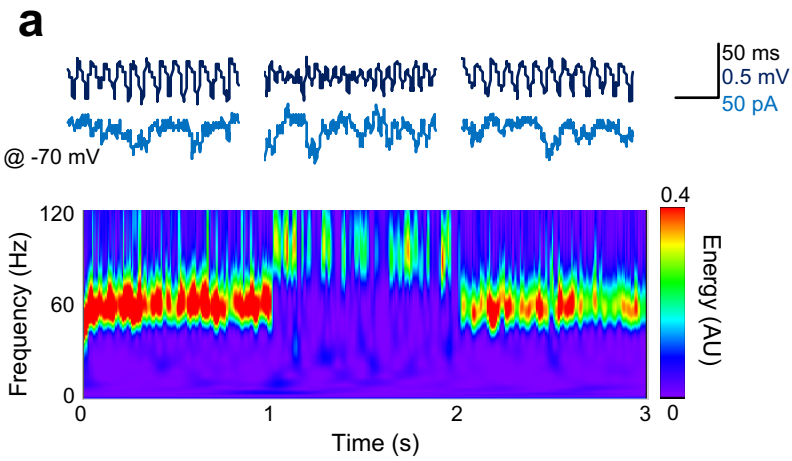
a
50 ms
0.5 mV
50 pA
@ -70 mV
120
60
0
Frequency (Hz)
0
1
2
3
Time (s)
0.4
0
Energy (AU)

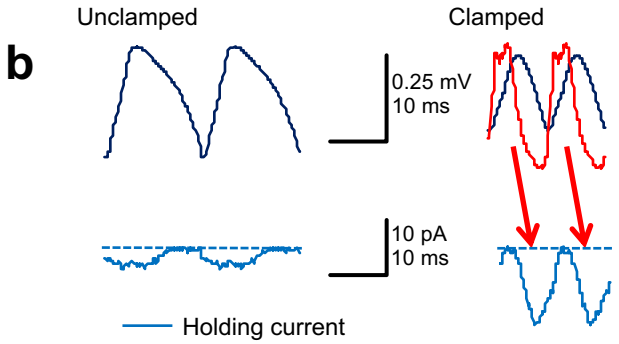
b
Unclamped
Clamped
0.25 mV
10 ms
10 pA
10 ms
Holding current

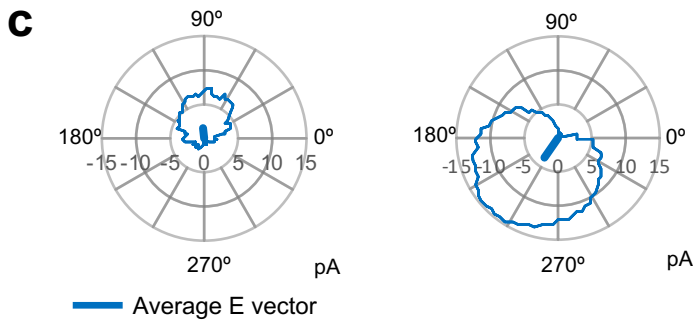
c
90°
180°
0°
270°
-15 -10 -5 0 5 10 15
pA
Average E vector

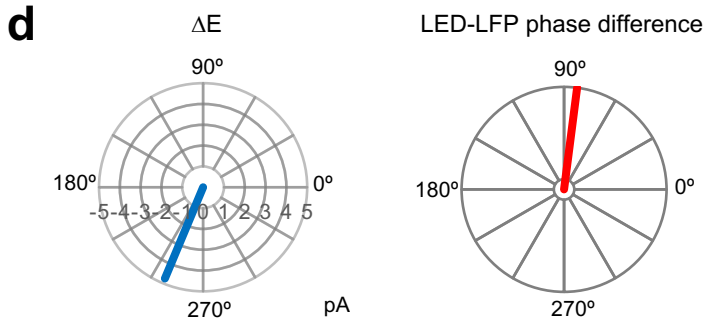
d
ΔE
LED-LFP phase difference
90°
180°
0°
270°
-5 -4 -3 -2 -1 0 1 2 3 4 5
pA

Fig. 5

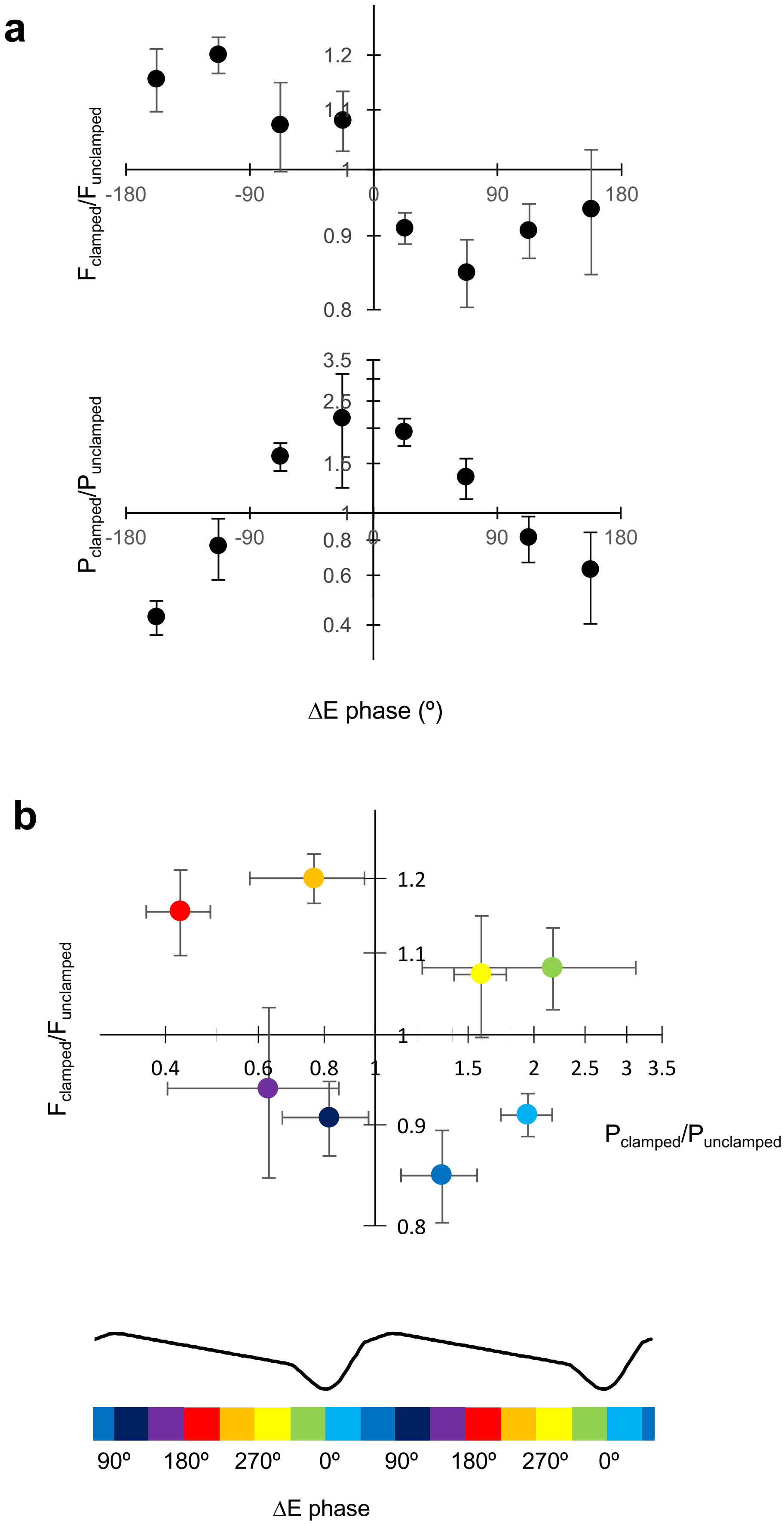
a
$F_{clamped}/F_{unclamped}$
$P_{clamped}/P_{unclamped}$
-180
-90
0
90
180
ΔE phase (º)
b
$F_{clamped}/F_{unclamped}$
$P_{clamped}/P_{unclamped}$
90º
180º
270º
0º
ΔE phase

Fig. 6

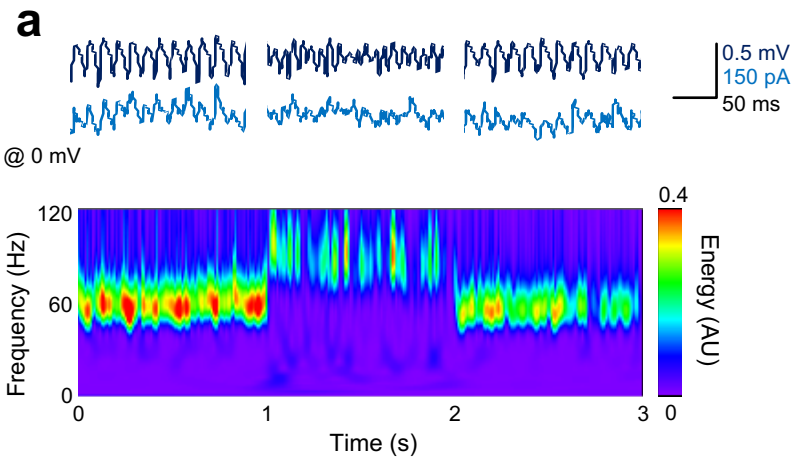
a
0.5 mV
150 pA
50 ms
@ 0 mV
120
60
0
Frequency (Hz)
0
1
2
3
Time (s)
0.4
0
Energy (AU)

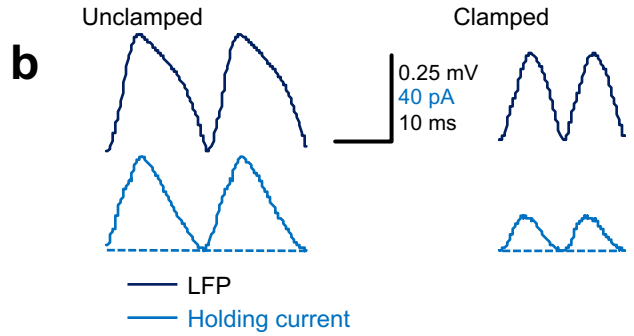
b
Unclamped
Clamped
0.25 mV
40 pA
10 ms
LFP
Holding current

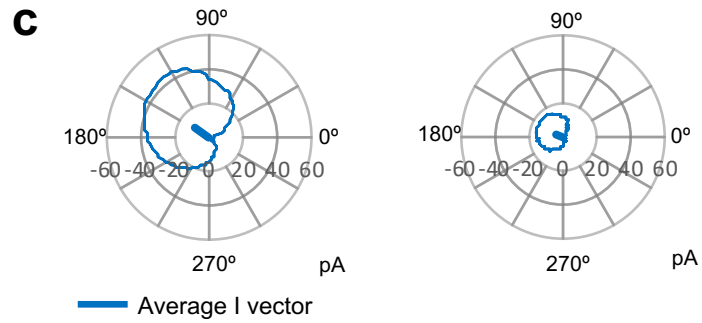
c
90º
180º
0º
270º
-60 -40 -20 0 20 40 60
pA
Average I vector

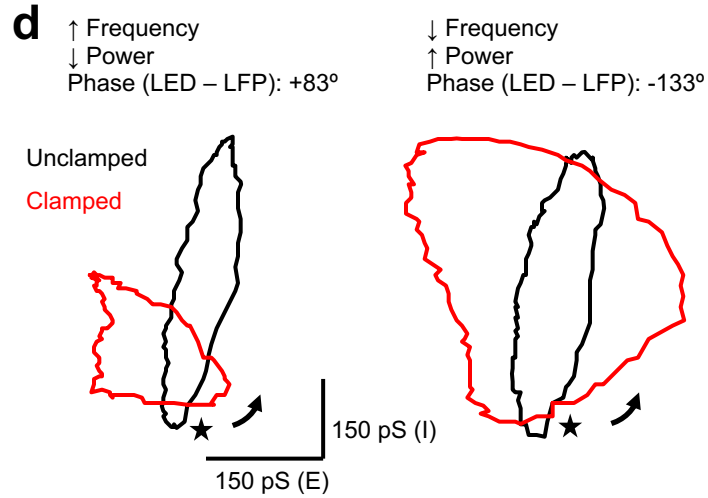
d
↑ Frequency
↓ Power
Phase (LED – LFP): +83º
↓ Frequency
↑ Power
Phase (LED – LFP): -133º
Unclamped
Clamped
150 pS (I)
150 pS (E)

Fig. 7